Tissue motion estimation using dictionary learning: application to cardiac amyloidosis

Nora Leïla Ouzir, Olivier Lairez, Adrian Basarab, Jean-Yves Tourneret

TISSUE MOTION ESTIMATION USING DICTIONARY LEARNING: APPLICATION TO CARDIAC AMYLOIDOSIS

Nora Ouzir[1], *Olivier Lairez*[2], *Adrian Basarab*[3], *Jean-Yves Tourneret*[1]

[1] University of Toulouse, INP-ENSEEIHT/IRIT/TeSA, 2 rue Camichel, 31071 Toulouse Cedex 7, France

[2] INSERM, UMR 1048, Institut des Maladies Métaboliques et Cardiovasculaires, CHU de Toulouse, Universit Paul Sabatier, Toulouse, France

[3] Université de Toulouse, IRIT, CNRS, Toulouse, France

ABSTRACT

Cardiac strain estimation from ultrasound images is an efficient tool for the diagnosis of cardiac diseases. This study focuses on cardiac amyloidosis, a pathology characterized by non-specific early symptoms such as the increased wall thickness. Recent clinical studies have demonstrated that patients with cardiac amyloidosis present an apex-to-base gradient longitudinal strain pattern, *i.e.*, a normal strain in apex and abnormally lower values for base segments. Existing cardiac motion estimation methods belong to three categories based on optical flow, speckle tracking and elastic registration. To overcome the ill-posedness of motion estimation, they use local parametric models (*e.g.*, affine) or global regularizations (*e.g.*, B-splines). The objective of this study is to evaluate a recently proposed cardiac motion estimation method based on dictionary learning on patients subjected to cardiac amyloidosis.

***Index Terms*—Cardiac motion estimation, dictionary learning, cardiac amyloidosis.**

I. INTRODUCTION

The amyloidoses are a rare group of diseases that result from extracellular deposition in organs and tissues of pathologic insoluble fibrillar proteins that self-assemble with highly ordered abnormal cross β-sheet conformation [1]. Fibrillar material derives from various precursor proteins and the classification of amyloidosis is based on the nature of the precursor plasma proteins that form the fibril deposits [2]. Acquired monoclonal immunoglobulin light-chain (AL) and transthyretin (TTR)-related (familial and wild-type/senile) diseases are the most frequent causes of cardiac amyloidosis [1]. The diagnosis of amyloid cardiomyopathy is usually difficult on the basis of noninvasive studies alone and almost invariably requires tissue confirmation. Biopsy procedures are not without risk of hemorrhage, possibly due to increased fragility of blood vessels or factor X deficiency. Regarding the prognostic value of the organ involvement pattern, a noninvasive test would be helpful in evaluating the extent of organ involvement in amyloid disease, thereby eliminating the risk of multiple biopsy procedures. Echocardiography is considered the gold standard for noninvasive detection of amyloid cardiomyopathy. However, echocardiography is not specific for cardiac amyloidosis and cardiac MRI is most of the time required for the non-invasive diagnosis, before histological confirmation. In fact, cardiac amyloidosis is manifested mainly by increased left ventricular myocardial thickness, which is a common echocardiographic finding, and can be related to a multitude of other cardiac disorders, such as aortic stenosis, hypertensive heart disease or hypertrophic cardiomyopathy. Among the etiologies leading to left ventricular hypertrophy, cardiac amyloidosis is one of most common and is a powerful independent risk factor for cardiovascular mortality [3]. Specifically, amyloid infiltration of the heart typically leads to a restrictive cardiomyopathy and progressive congestive heart failure and sudden death. Therefore, early diagnosis and specific management is key determinant in the prognosis of these patients. Furtheremore, recent studies suggest that regional patterns in longitudinal strain using two-dimensional speckle-tracking echocardiography would allow differentiating cardiac amyloidosis from other causes of left ventricular hypertrophy [4].

Cardiac motion estimation from ultrasound spatio-temporal images plays a key role in the assessment of strain measurements. Therefore, methods aiming at accurately estimating the heart motion have received a considerable attention in the literature. They mainly fall into three categories based on speckle tracking, optical flow and elastic registration. Speckle tracking consists in matching blocks of pixels from frames acquired at different time instants using standard similarity or dissimilarity metrics such as cross-correlation [5], sum of absolute differences (SAD) [6] or sum of squared differences (SSD) [7]. Optical flow methods are based on the pixel brightness constancy constraint. They estimate the motion fields using global [8] or local regularization models [9]. Finally, elastic registration methods estimate non-rigid geometric transformations (*e.g.*, represented on a B-spline basis [10], [11]) that align ultrasound images acquired at different times of the cardiac cycle.

This work was partially supported by the CIMI Labex, Toulouse, France, under grant ANR-11-LABX-0040-CIMI within the program ANR-11-IDEX-0002-02 and by ProSmart Solutions, 6-12 Rue Andras Beck 92360 Meudon, France.

The ill-posed nature of motion estimation, the complex local deformations of the heart and the intrinsic nature of ultrasound images affected by speckle noise are well-known issues that make the cardiac motion estimation difficult. In order to tackle these issues, existing methods integrate regularization approaches in the form of spatial smoothness [10], [11] or local parametric models (*e.g.*, affine model [9], [12]). However, this *a priori* knowledge is often application-independent, *i.e.,* it is not directly related to the cardiac motion nature. We have recently shown that using a sparsity-based regularization through trained dictionaries containing patterns of cardiac motion improves estimation accuracy compared to several state-of-the-art methods [13], [14]. The main objective of this paper is to show the effectiveness of this method in estimating apex-to-base gradient longitudinal strain patterns on patients subjected to cardiac amyloidosis.

The reminder of this manuscript is structured as follows. In the following section we provide a short overview of sparse representations through learned cardiac motion dictionaries. Section III resumes the cardiac motion estimation method used in this study. Finally, before concluding the paper, *in vivo* results are reported in Section IV.

II. OFFLINE CARDIAC MOTION DICTIONARY LEARNING

Sparse representations express a signal or image as a linear combination of a few elements of a dictionary. Their interest in image processing has been intensively studied in the literature, in a number of applications such as image denoising, inpainting or demosaicing. While a large variety of data-independent transforms exists (*e.g.*, wavelets, discrete cosine or Fourier transform), it has been shown that dictionaries learned from the data itself can be more efficient than the predefined ones [15].

In this work, two overcomplete dictionaries (*i.e.*, containing more atoms than the size of the motion patches to be sparsely coded) have been trained offline to capture typical patterns of vertical and respectively horizontal cardiac motions. The training process used motion patches extracted from simulated cardiac ultrasound image sequences with available ground-truth motion (see [16] for details about the ultrasound image simulation process). Mathematically, the calculation of the cardiac motion dictionary $\boldsymbol{D}$ translates into the following optimization problem

$$\min_{\boldsymbol{D},\boldsymbol{\alpha_p}} \sum\nolimits_p \|\boldsymbol{P}_p\boldsymbol{u} - \boldsymbol{D}\boldsymbol{\alpha}_p\|_2^2 \text{ subject to } \forall p,\ \|\boldsymbol{\alpha}_p\|_0 \leq K \quad (1)$$

where $\boldsymbol{P}_p \in \mathbb{R}^{n\times N}$ is a binary operator that extracts the pth patch of size n from the simulated motion field $\boldsymbol{u} \in \mathbb{R}^{N\times 1}$, $\boldsymbol{\alpha}_p \in \mathbb{R}^{q\times 1}$ is the corresponding sparse code, with K its maximum number of non-zero coefficients and $\boldsymbol{D} \in \mathbb{R}^{n\times q}$ is the dictionary to be estimated composed of a set of $q > n$ training elements called atoms. The optimization problem (1) was classically solved by iterating between a sparse coding step (estimating $\boldsymbol{\alpha}_p$ for a fixed $\boldsymbol{D}$) and a dictionary update step (estimating $\boldsymbol{D}$ for fixed sparse codes $\boldsymbol{\alpha}_p$). Note that (1) is solved twice, for the horizontal and vertical components of the cardiac motion field, respectively.

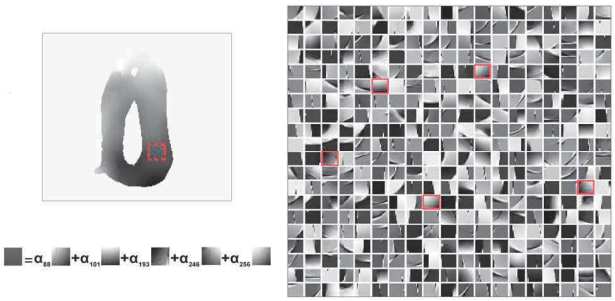

Fig. 1. Example of sparse representation of a cardiac motion patch in an overcomplete dictionary, expressed as the linear combination of 5 atoms.

Fig. 1 shows an example of a simulated cardiac motion field (horizontal component of the motion vectors) used in the offline dictionary learning process and the resulting atoms for the horizontal dictionary. As illustrated in this figure, a motion patch is only coded by a few atoms of the dictionary, namely 5 atoms in this example.

III. CARDIAC MOTION ESTIMATION

The cardiac motion estimation problem is formulated as the minimization of the cost function given below [13], [14]

$$\min_{\boldsymbol{\alpha}_p,\boldsymbol{u}} \left\{ E_{\text{data}}(\boldsymbol{u}) + \lambda_d \sum\nolimits_p \|\boldsymbol{P}_p\boldsymbol{u} - \boldsymbol{D}\boldsymbol{\alpha}_p\|_2^2 + \lambda_s \|\nabla \boldsymbol{u}\|_2^2 \right\} \quad (2)$$
$$\text{subject to } \forall p,\ \|\boldsymbol{\alpha}_p\|_0 \leq K$$

where E_{data} is the data fidelity term, the dictionary $\boldsymbol{D}$ results from the offline training described in the previous section and ∇ is the gradient operator, λ_d and λ_s are positive hyperparameters weighting the importance of the regularization terms with respect to the data attachment. The optimization problem (2) aims at estimating the cardiac motion field as a trade-off between the data fidelity and two regularizations imposing patchwise sparsity in the dictionary and spatial smoothness of the motion. Note that in this work the motion is estimated from B-mode images. As a consequence, the data fidelity term is based on the assumption of multiplicative Rayleigh-distributed speckle noise corrupting the envelope images (see [13], [17] for more details about the derivation of the likelihood function). To solve (2), we alternate between estimating the motion field $\boldsymbol{u}$ for fixed $\boldsymbol{\alpha}_p$ and a sparse coding, which consists in decomposing sparsely all motion patches $\boldsymbol{P}_p\boldsymbol{u}$ in the dictionary $\boldsymbol{D}$ [13], [14].

IV. *IN VIVO* RESULTS

The cardiac motion estimation method described previously was shown in [13], [14] to outperform several existing algorithms on the highly realistic simulations of B-mode

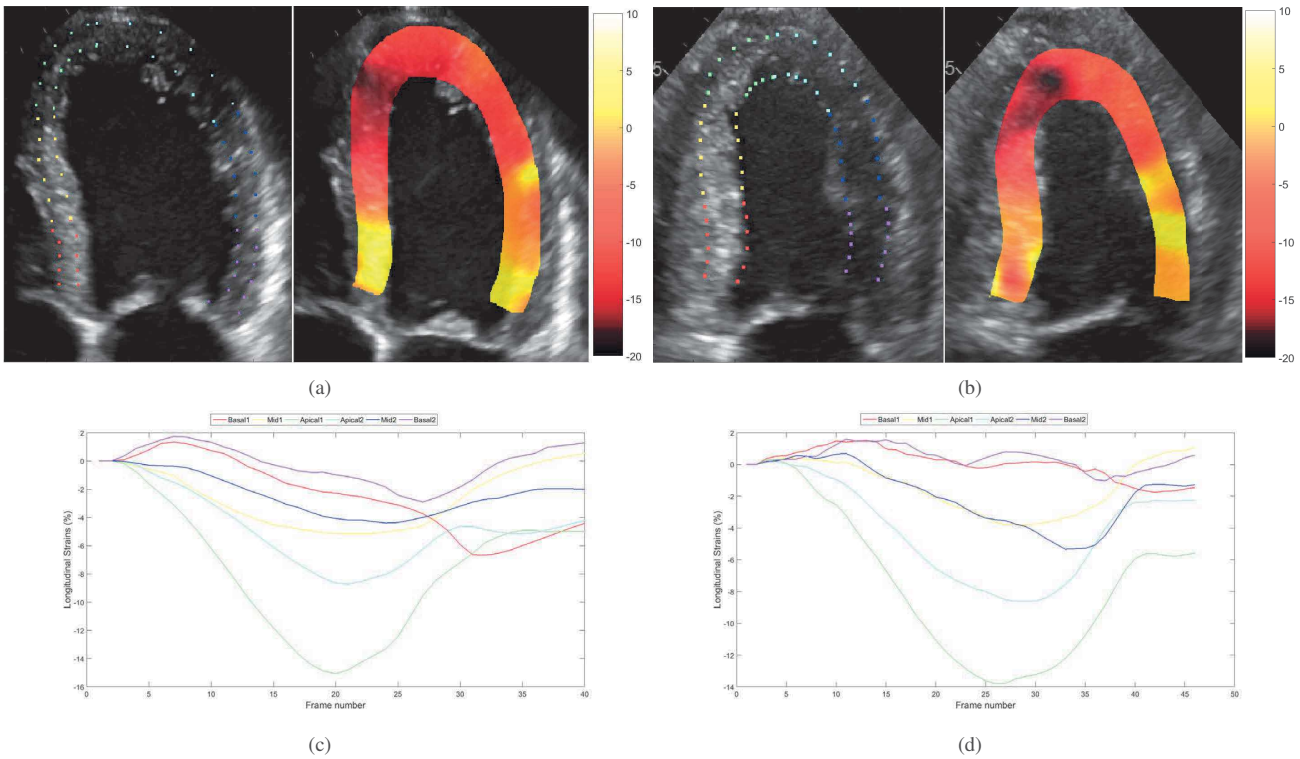

Fig. 2. *In vivo* longitudinal strain maps super-imposed to the B-mode images and strain curves over the cardiac cycle corresponding to the 6 myocardium segments. (a) and (c) correspond to patient 1, (b) and (d) correspond to patient 2.

ultrasound data (obtained using the method introduced in in [16]), including speckle tracking, the B-spline elastic registration studied in [11] and the monogenic phase-based optical flow [12].

In this paper, we evaluate its ability to estimate meaningful longitudinal strain maps for two patients suffering from cardiac amyloidosis. The long-axis view data was acquired by a specialist doctor using a GE Vivid E90 cardiovascular ultrasound system. For both patients, the motion was estimated over an entire cardiac cycle of 40 frames. The spatial smoothness hyperparameter was fixed to $\lambda_s = 0.75$ and λ_d was logarithmically increased at each iteration from 10^{-3} to 10^2. The size of the motion patches was set to 20×20 ($n = 400$), the sparsity parameter was fixed to $K = 5$ and the dictionary D had a redundancy of 1.5 ($q = 600$).

Using the estimated motion fields, longitudinal strain maps for the apical four-chambers view were calculated following the procedure studied in [16]. For a given frame k, the distance d_k between adjacent points uniformly chosen in the myocardium was measured. Strain values were then obtained relatively to the first frame of the cardiac cycle as

$$s_k = \frac{d_k}{d_0} - 1 \tag{3}$$

where d_0 is the distance between the points in the first frame of the cardiac cycle. The myocardium was manually segmented by the radiologist and further divided into 6 regions of interest for which an average strain value was computed.

Fig. 2 displays, for each patient, the initial points used for the longitudinal strain calculation, the strain curve evolution over a cardiac cycle for the 6 cardiac segments and an example of a longitudinal strain map super-imposed to the B-mode image. The strain maps shown in Fig. 2 correspond to the maximum deformation state of the heart, *i.e.,* the end systole. The results clearly highlight the apex-to-base gradient longitudinal strain pattern specific to cardiac amyloidosis. In particular, the maximum apical strain obtained at the end systole corresponds to normal values ranging from 15% to 20% of deformation, while it dramatically drops to abnormally low values (almost 0%) in the basis segments. The same behaviour can be observed from the mean strain over the whole cardiac cycle, highlighted by the two plots in Fig. 2 corresponding to the two patients considered in this study. We note that the mean strain values computed in each myocardium segment progressively decreases for the segments close to the myocardium basis. In particular, normal strain behaviour of the apex segments

and abnormally low strain variations of the basis segments over the cardiac cycle can be observed.

V. CONCLUSIONS

Cardiac amyloidosis is a severe cardiac pathology. The interest of echocardiography and in particular of longitudinal strain in its diagnosis has been recently highlighted. The objective of this paper was to evaluate the ability of a recently proposed cardiac motion estimation method to highlight the apex-to-base gradient longitudinal strain pattern specific to cardiac amyloidosis. Encouraging results were shown on two patients, and should be further confirmed through an extended study including more patients.

VI. REFERENCES

[1] R. H. Falk, R. L. Comenzo, and M. Skinner, "The systemic amyloidoses," *New England Journal of Medicine*, vol. 337, no. 13, pp. 898–909, 1997.

[2] J. D. Sipe, M. D. Benson, J. N. Buxbaum, S. ichi Ikeda, G. Merlini, M. J. M. Saraiva, and P. Westermark, "Amyloid fibril proteins and amyloidosis: chemical identification and clinical classification international society of amyloidosis 2016 nomenclature guidelines," *Amyloid*, vol. 23, no. 4, pp. 209–213, 2016.

[3] R. H. Falk, "Pondering the prognosis and pathology of cardiac amyloidosis," *JACC: Cardiovascular Imaging*, vol. 9, no. 2, pp. 139–141, 2016.

[4] D. Phelan, P. Collier, P. Thavendiranathan, Z. B. Popović, M. Hanna, J. C. Plana, T. H. Marwick, and J. D. Thomas, "Relative apical sparing of longitudinal strain using two-dimensional speckle-tracking echocardiography is both sensitive and specific for the diagnosis of cardiac amyloidosis," *Heart*, vol. 98, no. 19, pp. 1442–1448, 2012.

[5] V. Behar, D. Adam, P. Lysyansky, and Z. Friedman, "Improving motion estimation by accounting for local image distortion," *Ultrasonics*, vol. 43, no. 1, pp. 57–65, 2004.

[6] C. Kontogeorgakis, M. Strintzis, N. Maglaveras, and I. Kokkinidis, "Tumor detection in ultrasound B-mode images through motion estimation using a texture detection algorithm," in *Computers in Cardiology*. IEEE Comput. Soc. Press, 1994, pp. 117–120.

[7] F. Yeung, S. F. Levinson, and K. J. Parker, "Multilevel and motion model-based ultrasonic speckle tracking algorithms," *Ultrasound in Medicine & Biology*, vol. 24, no. 3, pp. 427–442, 1998.

[8] G. E. Mailloux, F. Langlois, P. Simard, and M. Bertrand, "Restoration of the velocity field of the heart from two-dimensional echocardiograms," *IEEE Trans. Med. Imaging*, vol. 8, no. 2, pp. 143–153, 1989.

[9] M. Suhling, M. Arigovindan, C. Jansen, P. Hunziker, and M. Unser, "Myocardial motion analysis from b-mode echocardiograms," *IEEE Trans. Image Process.*, vol. 14, no. 4, pp. 525–536, 2005.

[10] M. Ledesma-Carbayo, J. Kybic, M. Desco, A. Santos, M. Suhling, P. Hunziker, and M. Unser, "Spatio-temporal nonrigid registration for ultrasound cardiac motion estimation," *IEEE Trans. Med. Imaging*, vol. 24, no. 9, pp. 1113–1126, 2005.

[11] A. Myronenko, X. Song, and D. Sahn, "Maximum likelihood motion estimation in 3D echocardiography through non-rigid registration in spherical coordinates," in *Proc. 5th Int. Conf. Functional Imag. and Modeling of the Heart (FIMH'09)*, vol. 5528, Nice, France, June 2009, pp. 427–436.

[12] M. Alessandrini, A. Basarab, H. Liebgott, and O. Bernard, "Myocardial motion estimation from medical images using the monogenic signal," *IEEE Trans. Image Process.*, vol. 22, no. 3, pp. 1084–1095, 2013.

[13] N. Ouzir, A. Basarab, H. Liebgott, B. Harbaoui, and J.-Y. Tourneret, "Motion estimation in echocardiography using sparse representation and dictionary learning," *submitted to IEEE Trans. Image Process.*, 2017.

[14] N. Ouzir, A. Basarab, and J.-Y. Tourneret, "Cardiac motion estimation in ultrasound images using spatial and sparse regularizations," in *IEEE Int. Conf. Image Process.*, Beijing, China, Sept. 2017.

[15] J. Mairal, F. Bach, J. Ponce, and G. Sapiro, "Online dictionary learning for sparse coding," in *Proc. 26th Annu. Int. Conf. Mach. Learning (ICML '09)*, Montreal, Quebec, Canada, 2009, pp. 689–696.

[16] M. Alessandrini, B. Heyde, S. Queiros, S. Cygan, M. Zontak, O. Somphone, O. Bernard, M. De Craene, M. O'Donnell, and J. D'hooge, "Detailed evaluation of five 3D speckle tracking algorithms using synthetic echocardiographic recordings," *IEEE Trans. Med. Imaging*, vol. 35, no. 8, pp. 1915–1926, Aug. 2016.

[17] B. Cohen and I. Dinstein, "New maximum likelihood motion estimation schemes for noisy ultrasound images," *Pattern Recognition*, vol. 35, no. 2, pp. 455–463, 2002.